0026-895X/95/010160-12$3.00/0

MOLECULAR PHARMACOLOGY, 48:160–171 (1995).

Effects of *n*-Dodecylguanidine on A-Type Potassium Channels: Role of External Surface Charges in Channel Gating

JIAN-AN YAO, NINA C. SAXENA, M. REZA ZIAI, SHIUN LING, and GEA-NY TSENG

Department of Pharmacology, Columbia University, New York, New York 10032 (J.-A.Y., S.L., G.-N.T.), Department of Neurology, University of Michigan, Ann Arbor, Michigan 48104-1687 (N.C.S.), and American Cyanamid Company, Medical Research Division, Lederle Laboratories, Pearl River, New York (M.R.Z.)

Received January 26, 1995; Accepted March 20, 1995

SUMMARY

n-Dodecylguanidine (C_{12}-G) is an amphipathic compound with a guanidine moiety, which is positively charged at physiological pH, and a hydrophobic side chain. Its effects on an A-type K^+ channel clone (rKv1.4) expressed in *Xenopus* oocytes were examined. C_{12}-G caused a concentration-dependent (1–20 μM) positive shift in the voltage dependences of the following channel properties: activation, inactivation, rate of decay during depolarization, and rate of recovery from inactivation. C_{12}-G was effective when added to the bath solution but was without effect when applied to the cytoplasm of oocytes, indicating an extracellular site of action. The effects of C_{12}-G were antagonized by elevation of the extracellular Mg^{2+} concentration and by external guanidine ions but were augmented by lowering of the ionic strength of the external solution. C_{12}-G did not affect the instantaneous current-voltage relationship for rKv1.4 or the time constant of decay during strong depolarizations, when the voltage dependence of channel activation approached a plateau. Our observations suggest that C_{12}-G exerts its actions by causing a positive shift in the external surface potential around rKv1.4, without altering the ion permeation process or voltage-independent transition steps. In canine ventricular myocytes, C_{12}-G caused changes in the function of a native A-type K^+ channel similar to those seen with rKv1.4. However, C_{12}-G had negligible effects on the voltage dependence of the slow delayed-rectifier K^+ channel in the same cell type, suggesting that the actions of C_{12}-G are not nonspecific.

Cell membranes carry negative charges (surface charges) (1–8). The surface charges on or around ion channels may play an important role in modulating channel function and pharmacology (9–12). A local surface potential created by these charges can concentrate cations in the vicinity of channel pores, leading to an increase in current amplitude (13, 14). Negative surface potential adds a bias voltage to the electrical field sensed by "voltage sensors" of ion channels, thus influencing the voltage-dependent gating properties (2, 15). The negative surface potential can participate in concentrating or repelling charged toxins or drug molecules around ion channels, thus affecting their apparent sensitivity to these pharmacological agents (3, 16, 17).

In view of the important roles played by surface charges in modulating channel function, it is important to identify the distribution of surface charges on ion channels (10), i.e., carboxyl side chains of the proteins (5), *N*-glycosylation sites on the external surface (7), and phosphorylation sites on the internal surface (6). It is also important to identify the relationship between these surface charges and various functional domains of the channels, e.g., the gating apparatus and ion permeation pore. The availability of ion channel clones allows one to evaluate the contribution of different chemical groups to surface charges using mutagenesis techniques. What we need now are sensitive probes to study the impact on channel function of alterations of surface charges.

The effects of guanidine and *n*-alkylguanidine derivatives on membrane function have been studied by others previously (18–20). It has been suggested that these compounds can be adsorbed to the extracellular surface of cell membrane, causing a positive shift in the external surface potential. However, there have been no rigorous tests of the proposed mechanism of action. Neither has there been detailed electrophysiological characterization of the effects of guanidine derivatives on ion channel function. Here we describe the effects of C_{12}-G (structure shown in Table 3) on the properties of a mammalian A-type K^+ channel clone (rKv1.4)

This work was supported by Grants HL30557 and HL46451 from the National Heart, Lung, and Blood Institute, National Institutes of Health (G.-N.T.), by an Established Investigatorship from the American Heart Association (G.-N.T.), by a Grant-in-Aid from the American Heart Association/New York City Affiliate (G.-N.T.), and in part by support from Lederle, American Cyanamid.

ABBREVIATIONS: C_{12}-G, *n*-dodecylguanidine; TEA, tetraethylammonium; $V_{0.5}$, half-maximal voltage; $[Mg^{2+}]_o$, external magnesium concentration; V_t, test voltage; V_c, conditioning voltage; I_{to1}, transient outward K^+ current; I_{Ks}, slow delayed-rectifier K^+ current; V_h, holding voltage; K_{CG}, binding constant for *n*-dodecylguanidine to surface charges; K_{Mg}, binding constant for Mg^{2+} to surface charges; EGTA, ethylene glycol bis(β-aminoethyl ether)-*N*,*N*,*N*′,*N*′-tetraacetic acid; HEPES, 4-(2-hydroxyethyl)-1-piperazineethanesulfonic acid.

expressed in *Xenopus* oocytes (21). Specifically, we tested the idea that C_{12}-G can modulate the function of rKv1.4 by causing a positive shift in the external surface potential around the channel. We also describe the effects of C_{12}-G on a native A-type K^+ channel in canine ventricular myocytes and compare them with the effects on another voltage-gated K^+ channel in the same cell type (22). Our data suggest that guanidine derivatives may provide a unique pharmacological method to modify channel function with channel selectivity. Furthermore, our results have an even broader implication. *n*-Alkylguanidines may provide the sensitive probes we need to study the properties and distribution of surface charges on and around ion channels. Some of the data have appeared in abstract form (23).

Materials and Methods

In Vitro cDNA Transcription and Oocyte Preparation

The cDNA sequences of rKv1.4 (21) and its amino-terminal deletion mutant RHK1Δ3–25 (24) in pBluescript vector (Stratagene) were used to prepare DNA templates for *in vitro* cRNA synthesis. Supercoiled plasmid DNA was linearized with *Hind*III. The transcription reaction was carried out using a commercial kit (Promega), in the presence of a "cap" analogue and T7 RNA polymerase. For each transcription reaction, the quality of cRNA product was checked by denaturing agarose gel electrophoresis. The cRNA was resuspended in RNase-free water for microinjection.

Xenopus oocytes were released from follicular cell layers by collagenase treatment (type B; Boehringer Mannheim, Indianapolis, IN). Four to 6 hr after isolation, oocytes were microinjected with a cRNA solution (40–50 nl each), using a Drummond microdispenser and injection pipettes with beveled tips (tip opening diameter, ~5 μm). The oocytes were then incubated at 18° in an ND96 solution (composition given below), supplemented with penicillin (100 units/ml) and streptomycin (100 μg/ml). Membrane currents were studied 2–6 days after injection.

Canine Ventricular Cell Preparation

Single ventricular myocytes were isolated from canine left ventricle as described (22). Briefly, a wedge of the left ventricular free wall around the first branch of the left circumflex coronary artery was excised, and the coronary artery was cannulated. The tissue was perfused for 10–20 min with Ca^{2+}-free Tyrode's solution (composition given below) containing collagenase (type II; Worthington, Freehold, NJ), followed by mincing and trituration in the same medium to release single cells. After disaggregation, the cells were kept in a collagenase-free, Ca^{2+}-containing solution and used within 6–10 hr.

Electrophysiological Experiments

Oocyte experiments. The oocytes were placed in a tissue chamber and superfused at room temperature (23–25°) with a nominally Ca^{2+}-free ND96 solution (unless stated otherwise), at a rate of approximately 3 ml/min. This Ca^{2+}-free solution was used to minimize the interference from endogenous Ca^{2+}-activated Cl^- currents (25). Membrane currents were studied using the conventional, two-microelectrode, voltage-clamp technique, with an Axoclamp 2A amplifier (Axon Instruments, Foster City, CA). Both voltage and current electrodes were filled with 3 M KCl solution and had tip resistances of 1–2 MΩ. A grounded shield was placed between the two electrodes to decrease capacitance coupling. In some experiments, C_{12}-G or TEA was injected into oocytes. The intracellular injection device was essentially the same as that used for cRNA injection, except that a fine-tipped injection pipette (tip diameter, ≤2 μm) was used to minimize cellular injury.

Cardiac myocyte experiments. The cells were allowed to adhere to a poly-L-lysine-coated glass coverslip, which was placed on the bottom of a cell chamber mounted on the stage of an inverted Nikon microscope; the cells were continuously superfused with the bath solution at room temperature. The voltage clamp was carried out using the whole-cell variant of the patch-clamp method (26), with a List EPC-7 amplifier (List Medical, Eberstadt, Germany). Wide-tipped pipettes were made of Boralex glass (Rochester Scientific, Rochester, NY); the tip resistance was 0.6–1.2 MΩ when pipettes were filled with normal Tyrode's solution. In some experiments, C_{12}-G was applied intracellularly with a pipette perfusion device that allowed an exchange of solutions in the pipette tip (27). This allowed the control data and data acquired in the presence of C_{12}-G to be obtained from the same cell.

Data Acquisition and Analysis

For experiments with both oocytes and canine ventricular myocytes, the generation of voltage-clamp protocols and the acquisition of data were controlled by an IBM/AT-compatible computer through pClamp software (Axon Instruments), via a 12-bit digital/analog and analog/digital converter (TL-1 DMA Interface; Axon Instruments). Data were filtered at 2 kHz with an eight-pole Bessel filter (Frequency Devices, Haverhill, MA), digitized on-line at a sampling interval of 0.3–1 msec, and stored on diskettes for off-line analysis. Specific voltage-clamp protocols and data analyses are described in the figure legends. Two methods were employed for curve fitting. The first used the program PeakFit (Jandel Scientific, Corte Madera, CA) to fit the activation and inactivation curves and the time course of recovery from inactivation. The second method used the program Clampfit of pClamp to fit the time courses of current decay during depolarizations. Data are presented as mean ± standard deviation. Statistical significance was tested using paired or unpaired Student's *t* test.

The relationship between the concentration of Mg^{2+}, C_{12}-G, or guanidine and the $V_{0.5}$ of rKv1.4 inactivation was analyzed based on the diffuse bilayer surface charge theory (28). We assumed that these ions could bind to surface charges with different binding affinities. The relationship between $V_{0.5}$ and the binding ion concentration was fit with the Gouy-Chapman equation, as modified by Gilbert and Ehrenstein (eq. 3) (15), to estimate the following parameters: the average spacing between surface charges (D), the binding constant for ions binding to surface charges (K), and the $V_{0.5}$ value of rKv1.4 inactivation when all surface charges were bound (B). To accomplish this, D, K, and B were assigned guessed values and an iteration procedure was established by first solving eq. 3 for $V_{0.5}$ values at different binding ion concentrations, using bisection or Newton conjugate method (29). A subroutine provided by the QuickPak Scientific package (Crescent Software, West Redding, CT) was then used to minimize the difference between the calculated and observed relationships between $V_{0.5}$ and the binding ion concentration until estimates for D, K, and B were found that could reasonably describe the observed concentration-response relationship.

Solutions and Drugs

For experiments on oocytes, the control ND96 solution had the following composition: 96 mM NaCl, 2 mM KCl, 1.8 mM $CaCl_2$, 1.0 mM $MgCl_2$, 5 mM HEPES, 2.5 mM sodium pyruvate, pH 7.5 with NaOH. The Ca^{2+}-free ND96 solution was made by substituting $MgCl_2$ for $CaCl_2$. When the effects of elevation of $[Mg^{2+}]_o$ on channel properties were studied, the Ca^{2+}-free ND96 solution was mixed with a Ca^{2+}-free/Mg^{2+}-rich solution at different ratios to obtain the desired final $[Mg^{2+}]_o$. The Mg^{2+}-rich solution was made by replacing total NaCl (96 mM) in ND96 solution with 64 mM $MgCl_2$. In some experiments, the ionic strength of the external solution was lowered by replacing all NaCl in the ND96 solution with sucrose at 1.78 mM sucrose/1 mM NaCl. Modified ND96 solutions containing different concentrations of guanidine were made by mixing the Ca^{2+}-free ND96 solution with a Ca^{2+}-free/guanidine-rich solution at different ratios. The guanidine-rich solution was made by replacing all NaCl with 96 mM guanidine chloride.

For experiments on canine ventricular myocytes, the pipette solution had the following composition: 90 mM potassium aspartate, 20 mM KCl, 10 mM EGTA, 5 mM ATP (K^+ salt), 2.77 mM $MgCl_2$, and 10 mM HEPES, pH 7.3 with KOH. The control bath solution was normal Tyrode's solution, which had the following composition: 146 mM NaCl, 4 mM KCl, 2 mM $CaCl_2$, 0.5 mM $MgCl_2$, 5.5 mM dextrose, and 5 mM HEPES, pH 7.3 with NaOH. During data collection, tetrodotoxin (15–30 μM) and Mn^{2+} (2 mM) or nisoldipine (1 μM) were added to the bath solution to suppress Na^+ and Ca^{2+} channel currents, respectively.

The stock solutions of C_{12}-G and its analogues (see Table 3) were made in dimethylsulfoxide at 0.1 M and stored in aliquots at 4°. Before experiments, an aliquot of the stock solution was thawed and added to the external solution to reach the desired final concentration. Dimethylsulfoxide at the highest concentration used (0.02%, v/v) did not affect channel properties in any appreciable way.

Results

Effects of C_{12}-G on the Voltage Dependence of rKv1.4 Gating

Activation. Fig. 1A shows the voltage-clamp protocol used to determine the peak current-voltage relationship of rKv1.4. Under control conditions, rKv1.4 was activated by depolarization pulses to V_t values equal or positive to −50 mV. In the presence of 5 μM C_{12}-G, the threshold of activation of rKv1.4 was shifted from −50 to −30 mV. Furthermore, the peak current amplitude was smaller than control between −30 and +30 mV but larger than control at more positive voltages (Fig. 1B).

These effects of C_{12}-G on the peak current-voltage relationship of rKv1.4 were due to a positive shift in the voltage dependence of channel activation, as shown in Fig. 2. An estimate of the fraction of channels activated at the peak of the current at each V_t was obtained by dividing the peak current amplitude (as described in Fig. 1) by the instantaneous current amplitude (determined as described in Fig. 6) and normalizing this value to that at +50 mV. The activation curve for rKv1.4 was constructed by fitting the data with a double-sigmoidal function,

$$\text{Fraction activated} = A_1/(1 + \exp[(V_1 - V_t)/k_1]) + (1 - A_1)/(1 + \exp[(V_2 - V_t)/k_2]) \quad (1)$$

where A_1 and $(1 - A_1)$ are the fractions of channels activated in the more negative (component 1) and more positive (component 2) voltage ranges, V_1 and V_2 are the half-maximal activation voltages, and k_1 and k_2 are the slope factors of components 1 and 2, respectively. Table 1 summarizes the parameters of the control activation curve and the effects of C_{12}-G from six cells. Under control conditions, component 1 comprised the major fraction of channels activated (A_1 = 0.70 ± 0.07), with V_1 of −38.5 ± 1.9 mV and k_1 of 5.5 ± 0.5 mV. Component 2 accounted for 30%, with V_2 of +2.1 ± 5.6 mV and k_2 of 15.7 ± 1.8 mV (Table 1). The most important effect of C_{12}-G was a positive shift in V_1 (by 24 mV). C_{12}-G did not alter either the fraction of this component (A_1) or its slope factor (k_1). There was also a positive shift in V_2 and a reduction in k_2 of the minor component.

Inactivation. The voltage dependence of steady state inactivation of rKv1.4 was studied by a double-pulse protocol, as described in the legend to Fig. 1C. The relationship between the V_c and the fraction of channels remaining available for activation during the test pulse (I_t/I_{max}) was fit with a simple Boltzmann function,

$$I_t/I_{max} = 1/(1 + \exp[(V_c - V_{0.5})/k]) \quad (2)$$

where k is the slope factor. Fig. 2 shows the effects of C_{12}-G on the inactivation curve for rKv1.4 from a representative

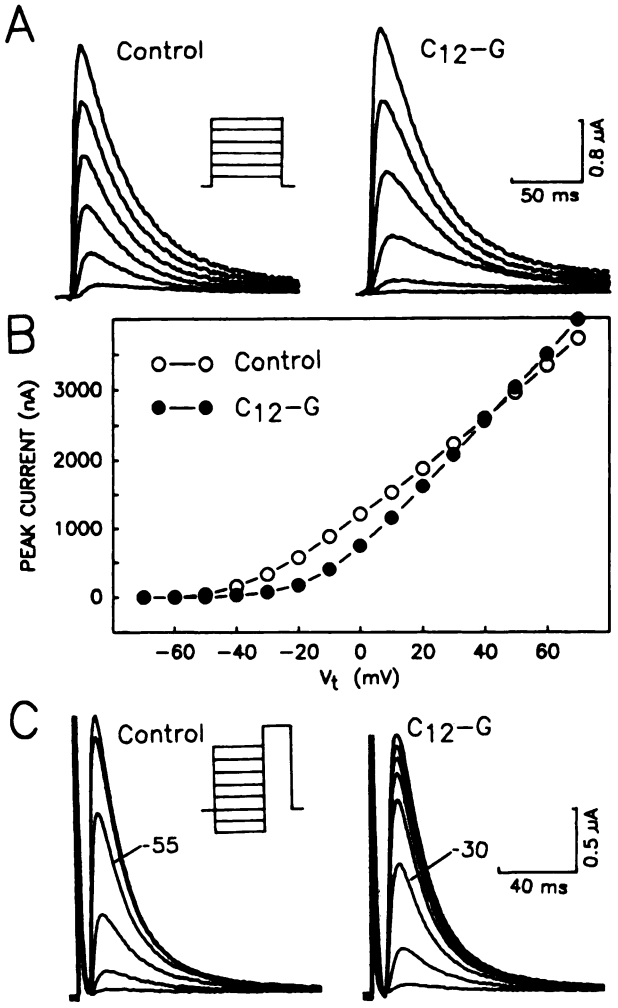

Fig. 1. Effects of C_{12}-G on the peak current-voltage relationship and the voltage dependence of inactivation for rKv1.4. A, Original current traces recorded in the absence (control) and presence of C_{12}-G (5 μM). The currents were induced by depolarization pulses from a V_h of −80 mV to V_t between −40 and +60 mV, in 20-mV increments, for 500 msec at an interval of 15 sec. *Inset*, voltage-clamp protocol. Linear capacitive and leak currents were subtracted using a template created by averaging 20 current traces induced by a step from −80 to −70 mV. B, Peak current-voltage relationships before and after addition of C_{12}-G, from the same experiment as in A. The amplitudes of peak currents were measured from the leak-subtracted traces as the differences between the outward peaks and the holding current level. C, Original current traces recorded before and after addition of C_{12}-G (5 μM), after various conditioning steps. *Inset*, double-pulse protocol used to determine the steady state inactivation curve for rKv1.4. From a V_h of −80 mV, a 2-sec conditioning step to voltages (V_c) ranging from −90 to −15 mV was followed by a test pulse to +20 mV for 500 msec. The double pulses were applied at an interval of 15 sec. The currents recorded at test pulses are shown. The V_c for the control traces shown ranged from −65 mV (largest amplitude) to −40 mV (smallest amplitude) in 5-mV increments. Approximately half of the channels were inactivated at a V_c of −55 mV. The V_c for the illustrated traces in the presence of C_{12}-G ranged from −55 to −20 mV in 5-mV increments. The $V_{0.5}$ occurred at about −30 mV.

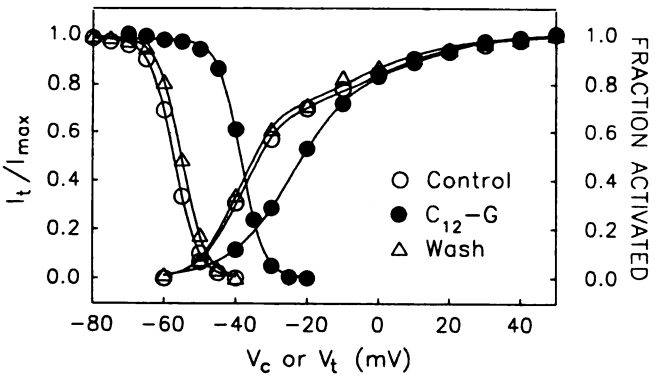

Fig. 2. Effects of C_{12}-G (5 μM) on the voltage dependences of activation and inactivation of rKv1.4 and the reversibility of these effects. The activation and inactivation curves were constructed as described in the text. The activation and inactivation curves shown were taken from the same cell. The half-maximal voltages for the major componento factivation (V_1) were −36.6, −22.3, and −39.6 mV before, during, and after exposure to C_{12}-G, respectively. The corresponding $V_{0.5}$ of inactivation values were −57.2, −38.6, and −55.1mV.

experiment. Under the control conditions, $V_{0.5}$ was −57.2 mV and k was 3.3 mV. C_{12}-G (5 μM) caused a positive shift in the inactivation curve for rKv1.4 ($V_{0.5}$ = −38.6 mV), without significantly altering the slope factor (k = 3.5). Data from six cells are summarized in Table 1. The C_{12}-G-induced positive shifts in the activation and inactivation curves of rKv1.4 were readily reversible (Fig. 2) and were concentration dependent (see Fig. 8B).

Effects of C_{12}-G on the Kinetics of rKv1.4 Gating

Inactivation. The time course of rKv1.4 inactivation during depolarization could be well described by a single-exponential function (Fig. 3A). The time constant was large at V_t close to the activation threshold (−40 mV) and decreased as V_t became more positive. The time constant attained a minimal asymptote in the voltage range positive to 0 mV (Fig. 3B). In the presence of C_{12}-G, the inactivation also followed a single-exponential time course (Fig. 3A). However, C_{12}-G increased the inactivation time constant at V_t negative to +30 mV. At more positive voltages, the time constant approached the same minimal asymptote as in control. Therefore, C_{12}-G shifted the curve relating the inactivation time constants and V_t in the positive direction by about 40 mV (Fig. 3B).

Activation. C_{12}-G also delayed the time to reach peak current of rKv1.4 (Fig. 4, A and B), suggesting a slowing of channel activation. However, the process of inactivation of the channel might interfere with the measurement of the rate of activation using time to peak current as an index. Therefore, we also tested the effects of C_{12}-G on the time to reach plateau current with a deletion mutant of rKv1.4 (RHK1Δ3–25), for which the fast inactivation process was prevented by deletion of amino acids 3–25 from the amino terminus (Fig. 4A, *right*) (24, 30). The slowing effect of C_{12}-G on the rate of channel activation was even more prominent in this inactivation-disrupted mutant. The delay in time to reach peak rKv1.4 current induced by C_{12}-G was observed over the entire voltage range examined (−10 to +70 mV) (Fig. 4B). In the same cell, C_{12}-G slowed the inactivation only in the voltage range up to +20 mV (Fig. 4C). At voltages positive to +30 mV, where the degree of channel activation approached a plateau both under control conditions and in the presence of C_{12}-G, the inactivation time constants were similar under these two conditions (Fig. 4C).

Recovery from inactivation (restitution). The restitution of rKv1.4 was studied by a double-pulse protocol (Fig. 5A). Under control conditions, this process could be well described by a single-exponential time course (Fig. 5B). The restitution process displayed a prominent voltage dependence; its time constant was decreased as the V_h became more negative (Fig. 5C). The restitution of rKv1.4 in the presence of C_{12}-G also followed an apparent single-exponential time course (Fig. 5B). However, C_{12}-G shortened the restitution time constant at all V_h values tested (−60 to −110 mV). The C_{12}-G-induced changes in the restitution time constants could be accounted for by a positive shift (by 17 mV) in the relationship between restitution time constant and V_h (Fig. 5C).

Effects of C_{12}-G on the Instantaneous Current-Voltage Relationship for rKv1.4

The properties of ion permeation of rKv1.4 and the effects of C_{12}-G were examined by measuring the instantaneous current-voltage relationship. Fig. 6A shows the double-pulse protocol used and the original tail current traces recorded under control conditions and in the presence of C_{12}-G (5 μM). The rKv1.4 tail currents were fit with a double-exponential function and extrapolated to the moment of repolarization to estimate the instantaneous current amplitudes through the channels. C_{12}-G did not significantly alter this current-voltage relationship for rKv1.4 (Fig. 6B). Similar observations were obtained in five other experiments.

Mechanism of C_{12}-G Action on rKv1.4

Sidedness of action. The experiments described above were done with C_{12}-G added to the bath solution. C_{12}-G was ineffective when delivered to the cytoplasm of oocytes (Fig. 7). This was done by pressure injection via a third intracellular pipette. The final cytoplasmic concentration of C_{12}-G was estimated by assuming that the oocytes were spheres with a diameter of 1 mm. Measurements were made 6–20 min after injections. At an estimated cytoplasmic concentration of 10 μM (n = 4) or even 200 μM (Fig. 7), C_{12}-G did not induce detectable shifts in the inactivation curve for rKv1.4. To check the effectiveness of the intracellular injection procedure, TEA was applied at an estimated cytoplasmic concentration of 5 mM by using the same technique. This led to a rapid suppression of rKv1.4 current (n = 4). Fig. 7, *inset*, shows an example of TEA injection, with a time constant of block development of 85 sec.

It has been previously suggested that the pharmacological actions of substituted guanidines arise from a positive shift in the external surface potential after adsorption of these compounds to the cell membrane (19, 20). We therefore studied the importance of external surface potential in the gating of rKv1.4 and its role in the actions of C_{12}-G. Three interventions were employed, i.e., increasing the external divalent cation concentration, reducing the ionic strength of the bath solution, and applying extracellular guanidine. The voltage dependence of rKv1.4 was monitored by its inactivation curve.

Effects of elevating the external divalent cation concentration on the actions of C_{12}-G. Although Ca^{2+} has been widely used to alter the surface potential, it was not

TABLE 1

Effects of C_{12}-G (5 μM) on the voltage dependences of activation and inactivation of rKv1.4

The activation curves were constructed in the following manner. For each of the cells studied, the peak current-voltage relationship (measured as described for Fig. 1, A and B) and the instantaneous current-voltage relationship (measured as described for Fig. 6) were determined from the same cell both under control conditions and in the presence of C_{12}-G. An estimate of the fraction of channels activated at the peak of the current at each V_t was obtained by dividing the peak current amplitude by the instantaneous current amplitude and normalizing this value to the value at +50 mV. The relationship between the fraction of channels activated and V_t was fitted with eq. 1, fraction activated = $A_1/(1 + \exp[(V_1 - V_t)/k_1]) + (1 - A_1)/(1 + \exp[(V_2 - V_t)/k_2])$, where A_1 is the fractional component activated in the negative voltage range; V_1 and k_1 are the half-maximal activation voltage and slope factor, respectively, for this component; and V_2 and k_2 are the corresponding parameters for the component activated in the more positive voltage range. The inactivation curves were determined based on the data generated by the double-pulse protocol described for Fig. 1C. The peak current amplitude (I_t) during each of the test pulses was measured and normalized to the maximum current amplitude (I_{max}) during a test pulse after a conditioning pulse of −90 to −80 mV (I_t/I_{max}). The relationship between I_t/I_{max} and V_c was fitted with eq. 2, $I_t/I_{max} = 1/(1 + \exp[(V_c - V_{0.5})/k])$, where k is the slope factor. Statistical analyses were by paired Student's t test.

Activation	A_1	V_1	k_1	V_2	k_2	n[a]
		mV	mV	mV	mV	
Control	0.70 ± 0.07	−38.5 ± 1.9	5.5 ± 0.5	2.1 ± 5.6	15.7 ± 1.8	6
C_{12}-G	0.72 ± 0.16	−14.9 ± 4.6[b]	6.4 ± 2.5	16.4 ± 9.7[c]	9.5 ± 2.8[d]	6

Inactivation	$V_{0.5}$	k	n
	mV	mV	
Control	−57.1 ± 2.2	3.3 ± 0.2	6
C_{12}-G	−33.4 ± 3.6[b]	3.4 ± 0.2	6

[a] n, number of measurements.
[b] $p < 0.001$.
[c] $p < 0.05$.
[d] $p < 0.01$.

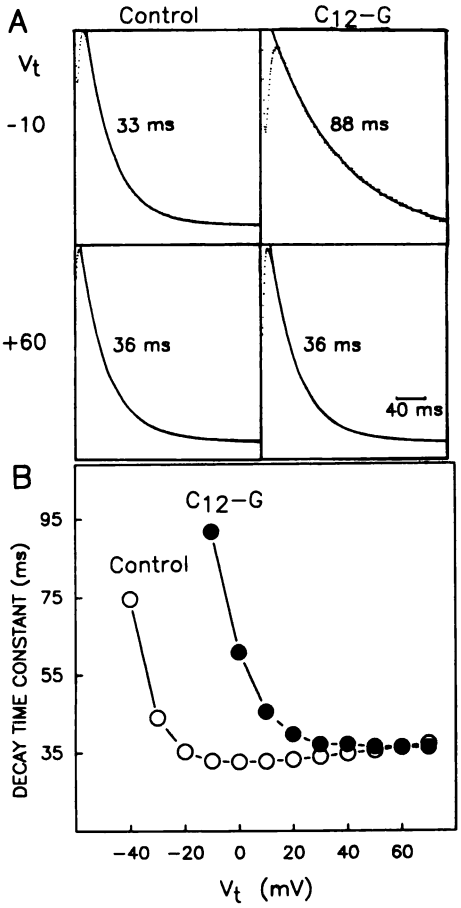

Fig. 3. Effects of C_{12}-G (5 μM) on the time course of rKv1.4 current decay during depolarization. The voltage-clamp protocol was as described for Fig. 1A. A, Currents (*dots*) recorded before (control) (*left*) and after C_{12}-G application (*right*), at the V_t indicated. The time courses of current decay were fit with a single-exponential function to estimate the decay time constants. The superimposed *curves* were calculated from the single-exponential function with the indicated decay time constants. B, Relationship between decay time constants and V_t before and after C_{12}-G application. Data were from the same experiment as in A. *Lines* connecting the data points were drawn by eye.

suitable for our purpose here because it could activate endogenous intracellular Ca^{2+}-activated Cl^- currents and interfere with rKv1.4 current measurement (25). A number of divalent cations tested blocked rKv1.4 channels (Ni^{2+}, Cd^{2+}, Co^{2+}, Ba^{2+}, and Mn^{2+}) (data not shown). Magnesium seemed to be the most inert in this respect and therefore was used to probe the presence of negative surface charges on or around rKv1.4 channels.

The inactivation curve for rKv1.4 was measured at different levels of $[Mg^{2+}]_o$. Elevating $[Mg^{2+}]_o$ from 2.8 mM (control) to >10 mM induced a concentration-dependent positive shift in the inactivation curve for rKv1.4 (Fig. 8A). This is consistent with the notion that there exist negative surface charges on or around the channels, creating an electrical field that influences the voltage dependence of channel gating (9, 11). Assuming that the negative charges are uniformly smeared over the external surface of the cell membrane and that Mg^{2+} ions could bind to the surface charges with a binding constant of K_{Mg}, the concentration-response relationship between Mg^{2+} and $V_{0.5}$ of inactivation was fit with the Gouy-Chapman equation, as modified by Gilbert and Ehrenstein (15),

$$D^2(1 + K_X[X]\exp[z_X F(B - V_{0.5})/RT]) = G\left/\left[\sum_{i=1}^{n} c_i(\exp[z_i F(B - V_{0.5})/RT] - 1)\right]^{0.5} \quad (3)$$

where D denotes the average spacing between external surface charges (in angstroms); K_X, [X], and z_X are the binding constant (in molar^{-1} units), concentration (in molar units), and valence, respectively, of the binding ion X (in this case X is Mg^{2+} and z_X is 2); B is the $V_{0.5}$ of rKv1.4 inactivation when all surface charges are bound ($V_{0.5} - B$ then is the external surface potential, in millivolts); G is a function of several physical constants and temperature [at 20°, G is 273 (Å^2/electronic charge)(M)$^{1/2}$]; n is the number of ion species in the external solution ($n = 6$ in our experiments); c_i and z_i are the concentration (in molar units) and valence, respectively, of

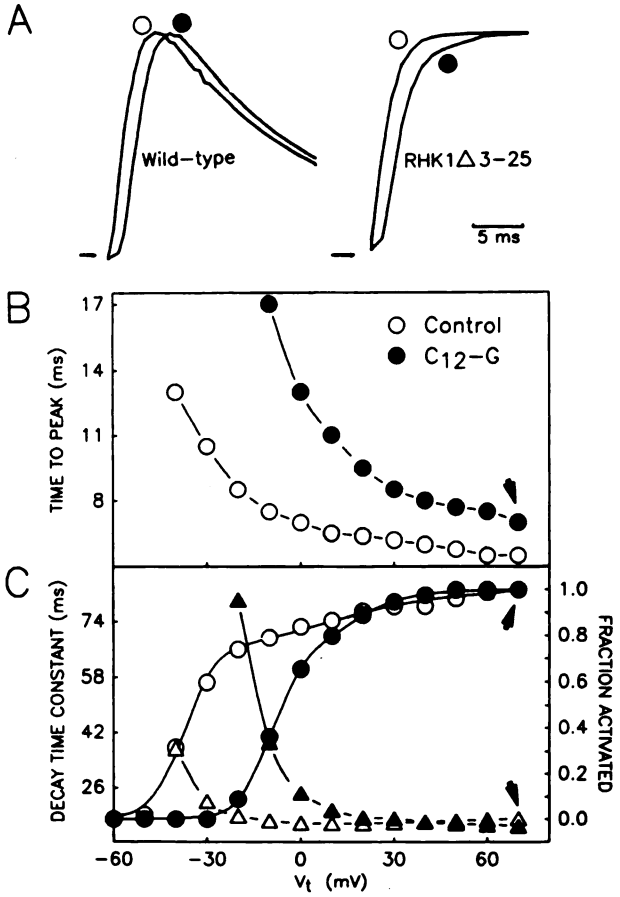

Fig. 4. Effects of C_{12}-G (5 μM) on the rate of rKv1.4 activation and comparison with its effects on the rate of rKv1.4 decay during depolarization. A, C_{12}-G delay of the time to reach peak current for rKv1.4 (wild-type channel) (*left*) and the time to reach plateau for a deletion mutant of rKv1.4 that lacks fast inactivation (RHKΔ3–25) (*right*). For both, two current traces recorded at +70 mV before (○) and after (●) C_{12}-G application are superimposed. Linear capacitive and leak currents have been subtracted. For the clarity of comparison, residual capacitive currents during the initial 2 msec (*left*) or 3 msec (*right*) after the start of depolarization have been omitted, and the gains of the current traces have been adjusted so that the peak or plateau current amplitudes before and after C_{12}-G application match each other. B, Relationships between the time to reach peak current for rKv1.4 (time to peak) and depolarization voltage (V_t) before (○) and after (●) C_{12}-G application. C, Relationships between V_t and the decay time constant (*triangles*, *left ordinate*) and the fraction of channels activated (*circles*, *right ordinate*) for rKv1.4 before (*open symbols*) and after (*filled symbols*) C_{12}-G application. Data in B and C were from the same experiment as shown in A, *left*. *Arrows*, at +70 mV the degree of channel activation and the rate of current decay were similar for control currents and currents measured in the presence of C_{12}-G, but the time to peak current was still prolonged in the presence of C_{12}-G.

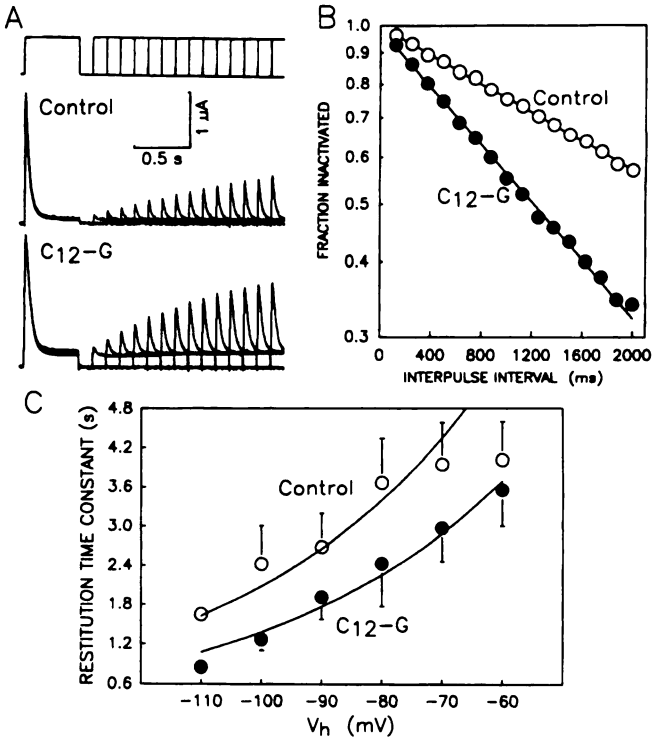

Fig. 5. Effects of C_{12}-G (5 μM) on the time course of restitution of rKv1.4. A, *Top*, voltage-clamp protocol used to determine the time course of restitution. Two depolarization pulses, each to +20 mV for 500 msec, were applied from a V_h ranging from −60 to −110 mV. The interpulse interval was varied from 125 to 4000 msec. The interval between the double pulses was 15 sec. *Middle* and *bottom*, original current traces recorded before (control) and after C_{12}-G application. The V_h of this experiment was −80 mV. B, Time courses of rKv1.4 restitution before and after C_{12}-G application, from the same experiment as shown in A. The fraction of channels remaining inactivated at the end of the interpulse interval was estimated by the reduction in the peak current amplitude during the second pulse, relative to the peak current amplitude during the first pulse. This value was plotted on a logarithmic scale against the interpulse interval. The time courses of restitution could be well described by a single-exponential function both under control conditions and in the presence of C_{12}-G, as reflected by the linear semilogarithmic plots. The *lines* superimposed on the data points in B were calculated based on the best-fit time constants of restitution, i.e., 3.6 and 1.8 sec for control and C_{12}-G, respectively. C, Summary of restitution time constants at different V_h values, before and after C_{12}-G (5 μM) application. Each data point represents an average from nine (−80 mV), seven (−60, −70, and −90 mV), five (−100 mV), or two (−110 mV) measurements (*standard deviation bars* are shown except for the data points at −110 mV). The relationship between the restitution time constant and V_h was fit with the following equation:

$$\tau(V_h) = \tau(0)\exp(zV_hF/RT) \quad (5)$$

where $\tau(V_h)$ and $\tau(0)$ are the restitution time constants at holding voltages of V_h *and 0 mV, respectively;* z denotes the voltage dependence of the restitution process; and F/RT is 0.0396 mV^{-1}. The *curves* in C were calculated from eq. 7 with $\tau(0)$ of 24.4 sec and 16.1 sec for control and C_{12}-G measurements, respectively, and a z value of 0.6 for both.

the ith ion in the solution; and F, R, and T have their usual meanings (F/RT = 0.04 mV^{-1}). The curve in Fig. 8A was calculated by eq. 3, with the following parameter values: D = 15.0 Å, B = +5.6 mV, and K_{Mg} = 1.8×10^{-2} M^{-1}.

The concentration-response relationship between C_{12}-G and $V_{0.5}$ for rKv1.4 inactivation was also quantified based on the surface charge theory, by fitting the data points with eq. 3. The curve in Fig. 8B was calculated with the following parameter values: D = 14.1 Å, B = +5.6 mV, and K_{CG} = 7.3×10^{4} M^{-1}. The values for D and B generated by fitting the concentration-response relationships for Mg^{2+} and C_{12}-G with eq. 3 were almost identical. However, the binding constants were dramatically different, with the binding affinity of C_{12}-G being >10^6 times of that of Mg^{2+}.

If both C_{12}-G and Mg^{2+} modified the voltage dependence of rKv1.4 by binding to overlapping populations of surface charges, their effects should not be additive. The data presented in Fig. 9A showed that such is the case. In this experiment, the oocyte was exposed to C_{12}-G twice, the first

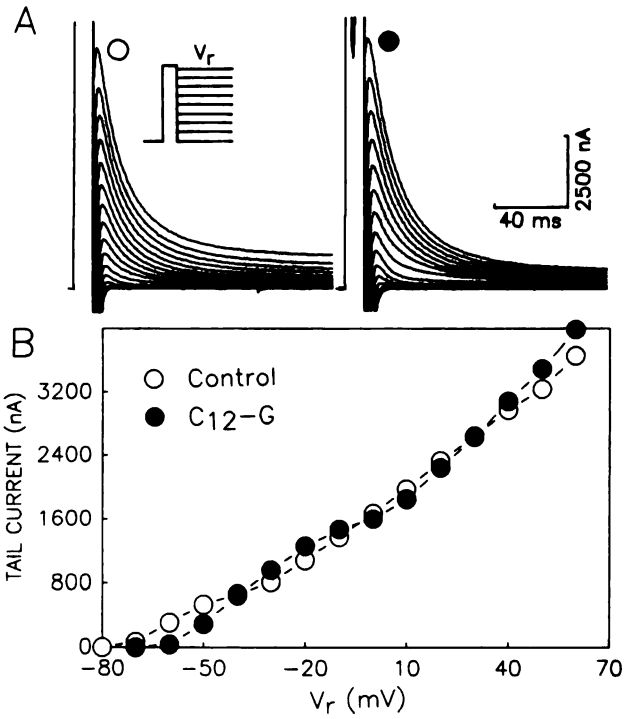

Fig. 6. Effects of C_{12}-G (5 μM) on the instantaneous current-voltage relationship for rKv1.4. A, Original tail current traces recorded before (*left*) and after (*right*) C_{12}-G application. *Inset*, voltage-clamp protocol; from a V_h of −80 mV a conditioning step to +70 mV for 10 msec was followed by a repolarization step to different voltages (V_r) for 250 msec. The double pulses were applied at an interval of 15 sec. The tail currents shown were recorded at a repolarization voltage of +50 to −80 mV, in 10-mV increments. B, Instantaneous current-voltage relationships from the same experiment as in A. The time courses of the tail currents were fitted with a double-exponential function. The amplitudes of the instantaneous currents were estimated by extrapolating the current to time 0 of repolarization.

time at $[Mg^{2+}]_o$ = 2.8 mM and the second at $[Mg^{2+}]_o$ = 21.8 mM. The inactivation curves determined in the presence of C_{12}-G under these two conditions were superimposable. The amount of $V_{0.5}$ shift induced by C_{12}-G was smaller at $[Mg^{2+}]_o$ of 21.8 mM (24.1 mV) than at 2.8 mM (33.7 mV). The effects of C_{12}-G (5 and 10 μM) on the inactivation curve for rKv1.4 at different levels of $[Mg^{2+}]_o$ (2.8, 21.8, and 65.8 mM) were studied in eight oocytes (Fig. 9B). Fig. 9B also shows the predicted shifts of $V_{0.5}$ under the same conditions. The calculation was based on the following equation, which was modified from eq. 3 to include two binding ions (Mg^{2+} and C_{12}-G):

$$D^2(1 + K_{Mg}[Mg^{2+}]\exp[2F(B - V_{0.5})/RT] + K_{CG}[C_{12} - G]\exp[F(B - V_{0.5})/RT]) = G\left[\sum_{i=1}^{n} c_i(\exp[z_iF(B - V_{0.5})/RT] - 1)\right]^{0.5} \quad (4)$$

The parameter values were taken from those in Fig. 8, as follows: D = 15 Å, B = 5.6 mV, K_{Mg} = 1.8 × 10^{-2} M^{-1}, and K_{CG} = 7.3 × 10^4 M^{-1}. The theoretical calculations provide a reasonable fit to some, although not all, of the experimental observations.

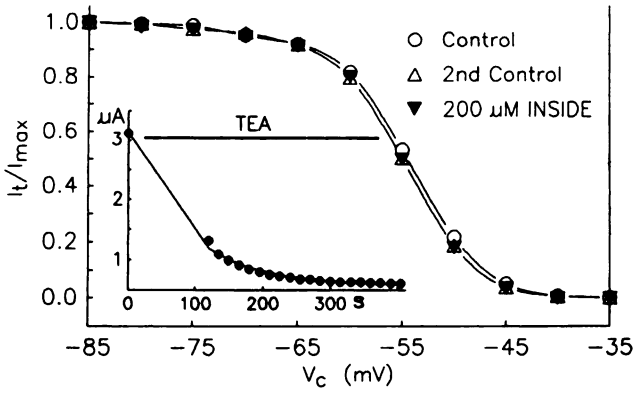

Fig. 7. Evidence that C_{12}-G affects rKv1.4 from the extracellular surface of the cell membrane. The inactivation curves for rKv1.4 were determined from the same oocyte under three conditions. *Control* and *2nd Control*, currents recorded before and after impalement with the injecting pipette, respectively. C_{12}-G was then pressure-injected intracellularly. Assuming that the oocyte was a sphere with a diameter of 1 mm, 100 nl of a 1 mM C_{12}-G solution were injected to reach an estimated final cytoplasmic concentration of 200 μM. The inactivation curve was measured 6 min after injection. *Inset*, time course of reduction of rKv1.4 current amplitude after intracellular injection of TEA (estimated final cytoplasmic concentration, 5 mM). The current amplitude was stable before TEA injection. Shortly after the last control data point (at time 0) was recorded, TEA was injected (*horizontal bar above data points*). The *curve* connecting the data points was calculated based on a single-exponential function, with an estimated time constant of 85 sec.

Effects of lowering external ionic strength on the actions of C_{12}-G. Lowering the ionic strength of the bathing solution can reduce the screening of surface charges by counter-ions, thereby enhancing the magnitude and range of the electrical field created by these charges (10, 11). If C_{12}-G exerted its effects by binding to external negative surface charges, lowering the ionic strength should amplify its actions by enhancing the electrostatic interactions between C_{12}-G and these charges. We therefore replaced all NaCl (96 mM) in the control ND96 solution with sucrose (ionic strength lowered from 0.11 to 0.014) and compared the effects of C_{12}-G under these two conditions.

Reducing the ionic strength accentuated the actions of C_{12}-G. Fig. 10 illustrates that C_{12}-G shifted the $V_{0.5}$ from −44.7 to −26.0 mV (a shift of 18.7 mV) in ND96 with normal ionic strength but from −50.4 to −15.8 mV (34.6 mV) in the medium with lower ionic strength. The observations were consistent among cells (Table 2). Therefore, these data support the hypothesis that C_{12}-G caused a positive voltage shift in the gating of rKv1.4 by binding to negative surface charges.

Effects of external guanidine on the actions of C_{12}-G. If C_{12}-G bound to negative surface charges by electrostatic interactions, its guanidine moiety (>90% protonated at physiological pH) (19) should be essential for its actions. We therefore tested the effects of guanidine ions on the voltage dependence of rKv1.4 gating and determined whether there were any interactions between C_{12}-G and guanidine ions. No appreciable effects on the voltage dependence of rKv1.4 gating were observed at guanidine concentrations below 10 mM. At higher concentrations (substituting guanidine for Na^+ ions in the external solution), guanidine induced a concentration-dependent (10–80 mM) positive shift in the activation and inactivation curves for rKv1.4 (Fig. 11A). These obser-

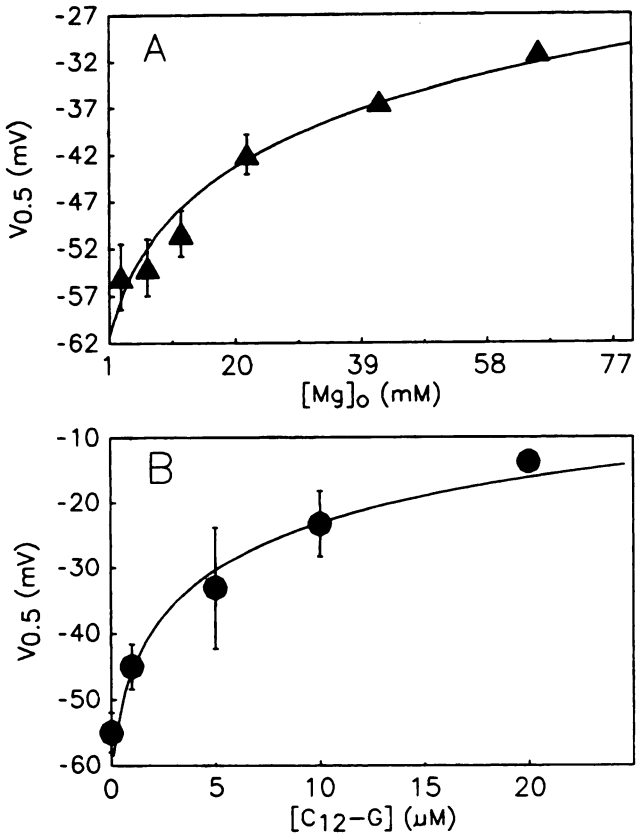

Fig. 8. A, Concentration-response relationship between $[Mg^{2+}]_o$ and the $V_{0.5}$ of rKv1.4. The $V_{0.5}$ was determined at different $[Mg^{2+}]_o$ values, ranging from 2.8 to 65.8 mM. Data points represent means of five to 14 measurements. Shown are means ± standard deviations. For data points without standard deviation bars, the size of the former is larger than that of the latter. The relationship between $V_{0.5}$ and $[Mg^{2+}]_o$ was fitted with equation 3. The *curve* super imposed on the data points was calculated from eq. 3 with the following parameter values: K_{Mg} = 1.8 × 10^{-2} M^{-1}, D = 15.0 Å, and B = +5.6 mV. B, Concentration-response relationship between C_{12}-G and $V_{0.5}$ for rKv 1.4 inactivation. The concentration of C_{12}-G ranged from 0 to 20 μM. Each data point represents mean from four measurements. The relationship between $V_{0.5}$ and the C_{12}-G concentration was fitted with eq. 3. The super imposed *curve* was calculated from eq. 3 with the following parameter values: K_{CG} = 7.3 × 10^4 M^{-1}, D = 14.1 Å, and B = +5.6 mV.

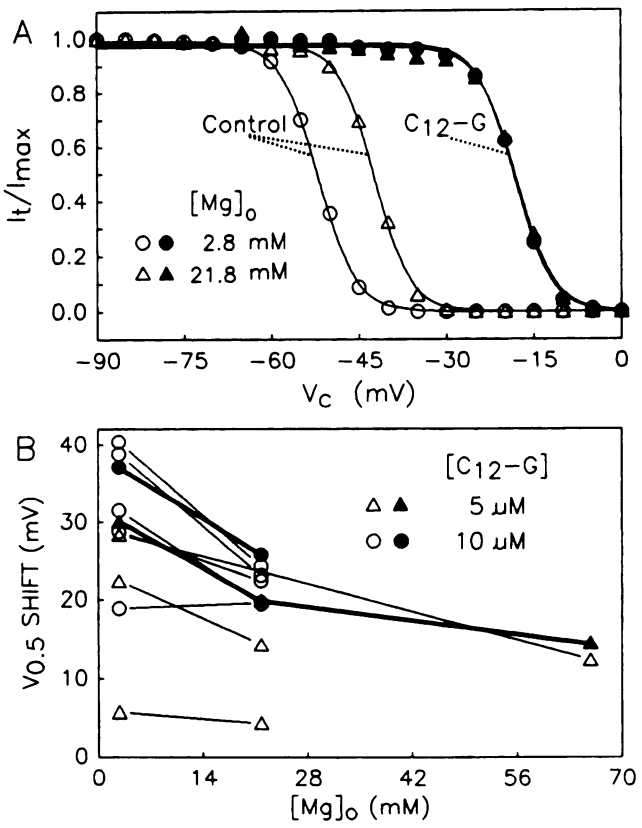

Fig. 9. Antagonism by elevation of $[Mg^{2+}]_o$ of the effect of C_{12}-G on the voltage dependence of inactivation of rKv1.4. A, Inactivation curves for rKv1.4 recorded from the same cell in the absence (*open symbols*) and presence (*filled symbols*) of C_{12}-G (10 μM), with $[Mg^{2+}]_o$ of either 2.8 mM (*circles*) or 21.8 mM (*triangles*). The sequence of the recording was as follows ($V_{0.5}$ in parentheses): $[Mg^{2+}]_o$ of 2.8 mM (−52.1 mV), $[Mg^{2+}]_o$ of 2.8 mM with C_{12}-G (−18.4 mV), washout of C_{12}-G and elevation of $[Mg^{2+}]_o$ to 21.8 mM (−42.2 mV), and $[Mg^{2+}]_o$ of 21.8 mM with C_{12}-G (−18.1 mV). B, Comparison between experimentally observed shifts in $V_{0.5}$ (*open symbols*) induced by C_{12}-G at different $[Mg^{2+}]_o$ values and those calculated based on the surface charge theory (*filled symbols*). Each pair of data points represent the $V_{0.5}$ shifts induced by C_{12}-G (*triangles*, 5 μM; *circles*, 10 μM), determined from the same cell at two $[Mg^{2+}]_o$ values (2.8 and 21.8 mM, or 2.8 and 65.8 mM). *Lines* connecting the data points were drawn for the sake of clarity. The theoretical values were calculated from eq. 4. The parameter values used for the calculation were as follows: D = 15.0 Å, B = +5.6 mV, K_{Mg} = 1.8 × 10^{-2} M^{-1}, and K_{CG} = 7.3 × 10^4 M^{-1}.

vations were consistent with previous reports (18, 20) and indicated that guanidine ions were more effective than Na^+ ions in screening or binding to negative surface charges. Guanidine induced a positive shift in $V_{0.5}$ of inactivation by 1.9 ± 0.7, 4.6 ± 2.8, 7.1 ± 2.7, and 10.5 ± 2.6 mV at 10, 20, 40, and 80 mM, respectively (n = 3–8 each). Fitting the concentration-response relationship between guanidine concentration and $V_{0.5}$ for rKv1.4 inactivation with eq. 3 generated the following parameter values: D = 16.0 Å, B = +5.6 mV, and K_{Gu} (binding constant for guanidine) = 5.4 × 10^{-1} M^{-1}. This suggests that the binding affinity of guanidine ion for surface charges is much weaker than that of C_{12}-G.

Fig. 11B illustrates the antagonism between C_{12}-G and guanidine ions in causing a positive shift in the inactivation curve for rKv1.4. C_{12}-G induced a shift in $V_{0.5}$ by 20.4 mV (from −52.7 to −32.3 mV) under control conditions but by only 7.8 mV (from −37.2 to −29.4 mV) when 80 mM guanidine was used to replace equimolar NaCl in the external solution. This was a consistent finding in four experiments performed (Table 2).

Effects of C_{12}-G Analogues on the Voltage Dependence of rKv1.4 Gating

The marked difference in potency between C_{12}-G and guanidine ions in inducing a positive voltage shift in rKv1.4 gating indicated that not only the guanidine moiety but also other parts of the molecule, e.g., the hydrophobic side chain, contributed to its binding to the cell membrane surface. We therefore tested the effects of modification of the guanidine moiety or the hydrophobic side chain of C_{12}-G on its potency to induce a voltage shift in rKv1.4 gating. Table 3 summarizes the results of these experiments. C_{12}-G (compound **1** in Table 3) at 20 μM caused a positive shift in $V_{0.5}$ for rKv1.4 inactivation by 36.5 ± 4.8 mV. Addition of a cyano group to the nitrogen of the guanidine (compound **6**) reduced the amount of $V_{0.5}$ shift by 75%, whereas fixing the guanidine as part of a bulky substituted pyrimidine structure (compound

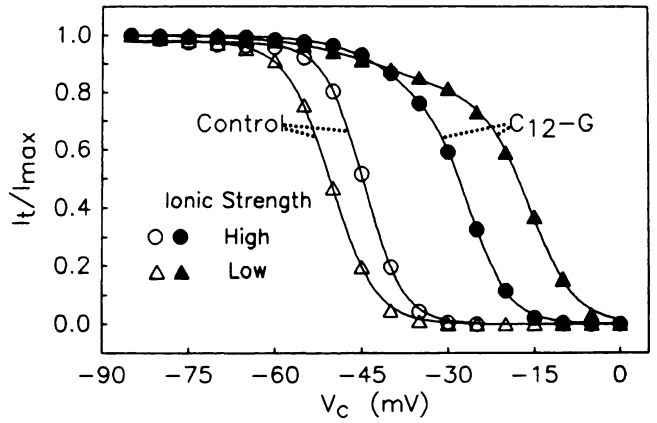

Fig. 10. Effects of C_{12}-G (10 μM) on the voltage dependence of inactivation of rKv1.4 at normal (high) or reduced external ionic strength. The high ionic strength external solution corresponded to the control ND96 solution, with an ionic strength of 0.11. The low ionic strength external solution was made by replacing all NaCl with sucrose (ionic strength, 0.014). The inactivation curves were determined from the same cell in the following order: high ionic strength with C_{12}-G (●), high ionic strength after washout of C_{12}-G (○), low ionic strength without C_{12}-G (△), and low ionic strength with C_{12}-G (▲). The inactivation *curves* in the absence of C_{12}-G were calculated from a simple Boltzmann function with the following best-fit parameter values: high ionic strength, $V_{0.5}$ = −44.7 mV and k = 3.4 mV; low ionic strength, $V_{0.5}$ = −50.4 mV and k = 3.9 mV. The relationships between I_t/I_{max} and V_c in the presence of C_{12}-G were fit with a double-sigmoidal function,

$$I_t/I_{max} = A_1/(1 + \exp[(V_c - V_1)/k_1]) + (1 - A_1)/(1 + \exp[(V_c - V_2)/k_2]) \quad (6)$$

where A_1 represents the fraction of channels inactivated in the more negative voltage range, with a $V_{0.5}$ of V_1 and a slope factor of k_1; V_2 and k_2 are the corresponding parameters for the component inactivated in the more positive voltage range. The *curves* were calculated from eq. 6 with the following parameter values: C_{12}-G at high ionic strength, A_1 = 0.33, V_1 = −37.2 mV, k_1 = 6.2 mV, V_2 = −26.0 mV, and k_2 = 3.3 mV; C_{12}-G at low ionic strength, A_1 = 0.22, V_1 = −41.4 mV, k_1 = 8.4 mV, V_2 = −15.8 mV, and k_2 = 3.9 mV.

7) reduced the potency by 90% ($p < 0.001$). Lengthening the alkyl side chain by one carbon (compound **2**) did not induce significant changes in the potency to cause a shift in $V_{0.5}$ ($p > 0.05$). However, shortening the alkyl side chain by two carbons (compound **4**) markedly reduced the $V_{0.5}$ shift (to 9.3 ± 5.2 mV). Adding an ethyl group to the first carbon of the alkyl chain (compound **3**) almost halved the amount of $V_{0.5}$ shift. Replacing the alkyl chain with a benzene ring (compound **5**) largely abolished the effect of C_{12}-G. Therefore, these structure-activity relationships support the notion that both the guanidine moiety and the hydrophobic side chain are important determinants of the efficacy of C_{12}-G in inducing a positive shift in the voltage dependence of rKv1.4 gating.

Effects of C_{12}-G on Native K^+ Channels in Canine Ventricular Myocytes

To better understand the mechanism of action of C_{12}-G on ion channels, we studied the effects of C_{12}-G on native K^+ channels in canine ventricular myocytes. In these myocytes, membrane depolarization activates currents through two major K^+ channels, the transient, outward or A-type K^+ channel (I_{to1}) and the slow delayed-rectifier K^+ channel (I_{ks}) (22). When I_{to1} was recorded, tetrodotoxin (15–30 μM) and Mn^{2+} (2 mM) or nisoldipine (1 μM) were used to suppress Na^+ and Ca^{2+} channel currents, respectively. At the end of the experiments, 4-aminopyridine (3 mM) was added to inhibit I_{to1}. I_{to1} was measured from the 4-aminopyridine-sensitive current as the difference between the outward peak current and the current level 200 msec after the start of depolarization.

TABLE 2

Effects of lowering of external ionic strength or addition of guanidine on the C_{12}-G-induced positive shift in the $V_{0.5}$ of rKv1.4

The cells were exposed to C_{12}-G twice, the first time before and the second time after the application of the intervention (lowering the external ionic strength or adding guanidine). The positive shifts in the $V_{0.5}$ of rKv1.4 induced by C_{12}-G under these two conditions are shown.

Cell number	C_{12}-G concentration	$V_{0.5}$	
		High ionic strength[a]	Low ionic strength[b]
	μM	mV	
1	10	28.3	32.6
2	10	29.4	31.0
3	10	24.4	27.1
4	10	18.7	34.6
5	10	29.3	39.4

Cell number	C_{12}-G concentration	$V_{0.5}$	
		0 mM Guanidine	80 mM Guanidine
	μM	mV	
1	5	15.8	10.6
2	10	34.6	14.5
3	5	17.0	7.4
4	5	20.4	7.8

[a] Ionic strength was calculated according to the following equation: ionic strength = $[\Sigma_{i=1}^{n}(c_i z_i^2)]/2$, where n is the total number of ion species in the external solution (n = 6) and c_i (in M) and z_i are the concentration and valence, respectively, of the ith ion. The high ionic strength solution corresponded to the control ND96 solution, whereas the low ionic strength solution was made by replacing all NaCl with sucrose (1.78 mM sucrose/1 mM NaCl).

[b] The inactivation curves in the presence of C_{12}-G were fitted with a double-sigmoidal function (eq. 6). The major component whose inactivation occurred in the more positive voltage range was taken as the C_{12}-G-modified component, and its $V_{0.5}$ was used to calculate the amount ofvoltage shift induced by C_{12}-G.

Fig. 12 compares the activation and inactivation curves for I_{to1} in controls and after application of C_{12}-G (20 μM). C_{12}-G induced a positive shift in $V_{0.5}$ of inactivation by 6.3 mV and a positive shift in the half-maximal voltage for the major component of activation (V_1) by 9.5 mV. The effects of C_{12}-G on the voltage dependence of activation of I_{to1} were examined in seven myocytes. C_{12}-G shifted V_1 by 4.0 ± 2.2 mV at 10 μM (n = 4, $p < 0.05$, paired t test) and by 8.7 ± 2.2 mV at 20 μM (n = 3, $p < 0.02$). C_{12}-G shifted the $V_{0.5}$ for I_{to1} inactivation by 8.3 ± 1.4 mV at 10 μM (n = 7, $p < 0.001$). These effects of C_{12}-G on the voltage dependence of gating of the native A-type K^+ channel were similar to those on rKv1.4 expressed in oocytes. Also, similarly to the effects on rKv1.4 as shown in Figs. 3 and 5, C_{12}-G increased the time constant of I_{to1} decay during depolarization at +10 and +20 mV, but not at more positive voltages, and accelerated the restitution of I_{to1} at −80 mV (data not shown). Furthermore, C_{12}-G modulated I_{to1} function from the extracellular side of the cell membrane, because in two myocytes intracellular dialysis with a pipette solution containing 100 μM C_{12}-G did not cause an appreciable shift in the inactivation curve for I_{to1}. Therefore, the actions of C_{12}-G on I_{to1} in canine ventricular myocytes were qualitatively similar to those on rKv1.4 in oocytes, although the latter was more sensitive than the former. These simi-

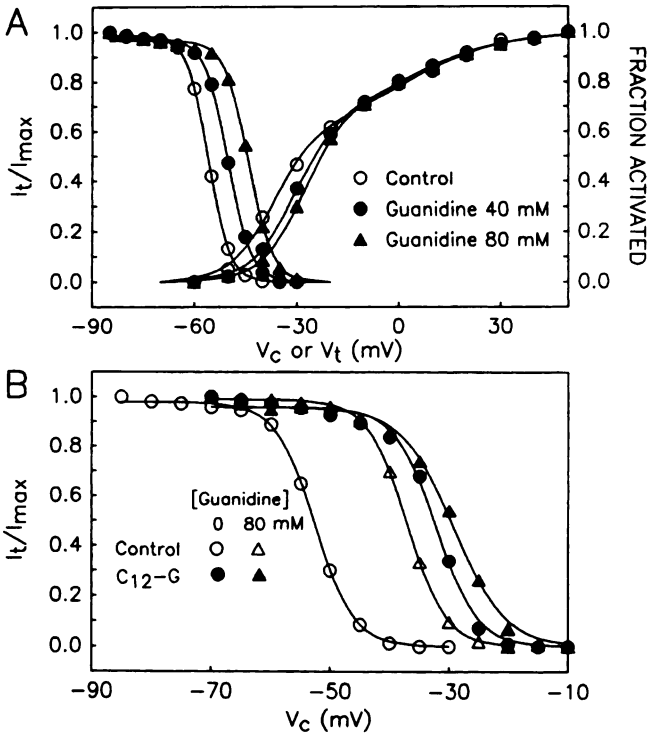

Fig. 11. A, Effects of guanidine on the voltage dependences of activation and inactivation of rKv1.4. The format and data analyses were the same as those described for Fig. 2. The activation *curves* superimposed on data points were calculated from the double-sigmoidal function (eq. 1) with the following best-fit parameter values: control, A_1 = 0.57, V_1 = −36.9 mV, k_1 = 6.0 mV, V_2 = +0.3 mV, and k_2 = 14.3 mV; 40 mM guanidine, A_1 = 0.61, V_1 = −30.7 mV, k_1 = 6.1 mV, V_2 = +1.0 mV, and k_2 = 14.6 mV; 80 mM guanidine, A_1 = 0.68, V_1 = −27.8 mV, k_1 = 6.1 mV, V_2 = +7.3 mV, and k_2 = 13.0 mV. The inactivation *curves* were calculated from the simple Boltzmann equation (eq. 2) with the following parameter values: control, $V_{0.5}$ = −55.9 mV and k = 3.1 mV; 40 mM guanidine, $V_{0.5}$ = −50.2 mV and k = 3.4 mV; 80 mM guanidine, $V_{0.5}$ = −44.2 mV and k = 3.5 mV. B, Effects of guanidine on the shift in $V_{0.5}$ induced by C_{12}-G (5 μM). The inactivation curve for rKv1.4 was determined from the same cell in the following sequence ($V_{0.5}$ in parentheses): control (−52.7 mV) (○), C_{12}-G (−32.3 mV) (●), washout of C_{12}-G and addition of 80 mM guanidine (−37.2 mV) (△), and 80 mM guanidine with C_{12}-G (−29.4 mV) (▲).

larities suggest that C_{12}-G might modulate I_{to1} function by the same mechanism as that described for rKv1.4.

We also tested the effects of C_{12}-G on I_{Ks} in five myocytes. One example is shown in Fig. 13. In contrast to the clear effects of C_{12}-G on I_{to1}, this agent did not seem to shift the voltage dependence of I_{Ks} gating. As shown in Fig. 13, the amplitude of I_{Ks} did not reach a plateau during 5-sec depolarization. Therefore, we could not measure the steady state activation curve. However, because C_{12}-G did not change the time course of I_{Ks} activation, the "isochronal" activation curve we used to compare the voltage dependence of channel activation before and after C_{12}-G application was valid. The half-maximal voltage for I_{Ks} activation was altered by C_{12}-G by −2.3 ± 5.8 mV at 10 μM (n = 3, $p > 0.5$) and by 1.9 ± 2.7 mV at 20 μM (n = 3, $p > 0.2$).

Discussion

The major findings of this study are as follows. 1) C_{12}-G caused a positive shift in the voltage dependences of rKv1.4 activation, inactivation, rate of decay during depolarization, and rate of recovery from inactivation. 2) These effects were exerted from the extracellular side of the cell membrane. 3) The effects of C_{12}-G on the voltage dependence of rKv1.4 inactivation were antagonized by elevation of $[Mg^{2+}]_o$ or by extracellular guanidine ions and were accentuated by decreases in the external ionic strength. 4) C_{12}-G caused changes in the function of a native A-type K^+ channel in canine ventricular myocytes similar to those for rKv1.4. However, C_{12}-G did not cause voltage shifts in the gating of a slow delayed-rectifier channel in the same cell type.

C_{12}-G is an amphipathic compound with a positively charged guanidine moiety and a hydrophobic side chain. There are several possible mechanisms by which such a molecule can modulate ion channel function in the cell mem-

TABLE 3

Comparison of the positive shifts in $V_{0.5}$ of rKv1.4 inactivation induced by various substituted guanidines

Compounds 1–5 have the following structures (R as specified in the table):

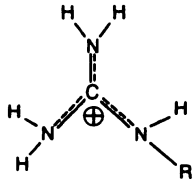

The positive shift in the $V_{0.5}$ of rKv1.4 inactivation induced by 20 μM of each substituted guanidine was determined. Values are mean ± standard deviation of n measurements.

Compound	Structure	Shift in $V_{0.5}$	n
		mV	
1	R = $-C_{12}H_{25}$	36.5 ± 4.8	4
2	R = $-C_{13}H_{27}$	27.1 ± 6.2	3
3	R = $-CH(C_2H_5)-C_{11}H_{23}$	19.7 ± 4.8[a]	3
4	R = $-C_{10}H_{21}$	9.3 ± 5.2[b]	3
5	R = $-CH_2-$ ⬡	2.2 ± 0.7[b]	3
6	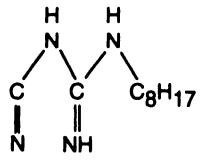	8.8 ± 0.4[b]	3
7	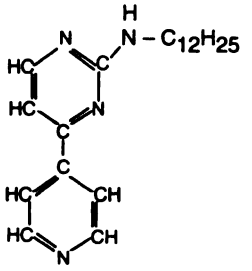	3.7 ± 1.3[b]	3

[a] $p < 0.01$, relative to the $V_{0.5}$ shift induced by compound 1 (C_{12}-G), by unpaired Student's t test.
[b] $p < 0.001$.

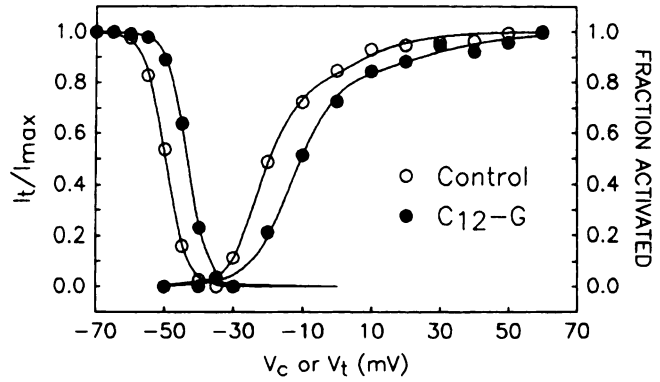

Fig. 12. Effects of C_{12}-G (20 μM) on the voltage dependences of activation and inactivation of I_{to1}. The activation curves were constructed in the same manner as that described for rKv1.4. The activation *curves* superimposed on the data points were calculated from eq. 1, using the following best fit parameter values: control, A_1 = 0.63, V_1 = −22.6 mV, k_1 = 3.9 mV, V_2 = −2.7 mV, and k_2 = 11.4 mV; C_{12}-G, A_1 = 0.78, V_1 = −13.1 mV, k_1 = 5.8 mV, V_2 = +21.7 mV, and k_2 = 14.6 mV. The inactivation curves were determined based on the data generated by the double-pulse protocol as described for rKv1.4. The inactivation *curves* were calculated from eq. 2 with the following parameter values: control, $V_{0.5}$ = −49.8 mV and k = 3.0 mV; C_{12}-G, $V_{0.5}$ = −43.5 mV and k = 2.9 mV.

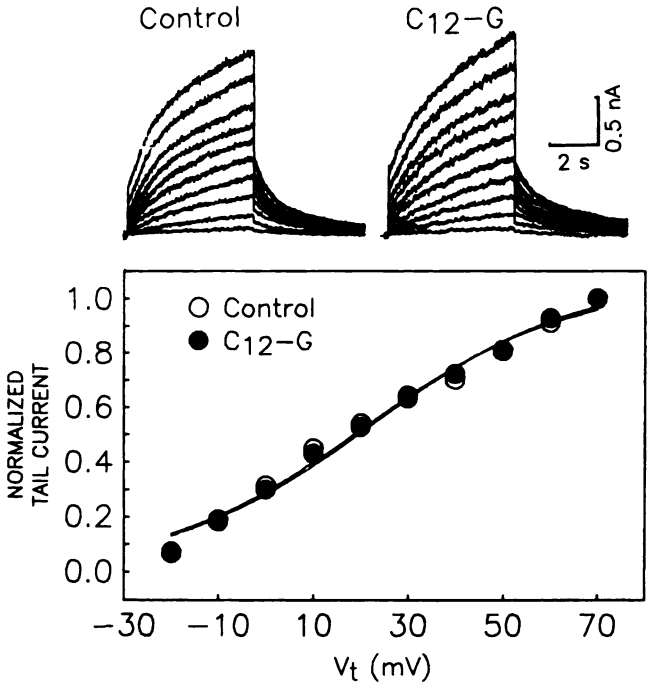

Fig. 13. Lack of effects of C_{12}-G (10 μM) on I_{Ks}. *Top*, original current traces recorded before (*left*) and during (*right*) exposure to C_{12}-G. The voltage-clamp protocol used a V_h of −30 mV, with depolarization to V_t of −20 to +70 mV in 10-mV increments for 5 sec, followed by repolarization to −30 mV for 5 sec; the interval between pulses was 25 sec. *Bottom*, tail current-voltage relationships from the same experiment. The amplitudes of outward tail currents were measured as the differences between the outward peaks and the holding current at −30 mV and were normalized to those after V_t = +70 mV. The current-voltage relationships were fit with a Boltzmann function to estimate the half-maximal activation voltage ($V_{0.5}$) and the slope factor (k), as follows: normalized tail current = $1/(1 + \exp[(V_{0.5} - V_t)/k])$. The *curves* were calculated using this equation with the following parameter values: control, $V_{0.5}$ = +21.1 mV and k = 21.6 mV; C_{12}-G, $V_{0.5}$ = +22.6 mV and k = 21.7 mV.

brane. First, an amphipathic compound can have "detergent effects" or alter the "membrane fluidity." This mechanism predicts that the effects of the amphipathic compound should not manifest channel selectivity. This is not the case for C_{12}-G, because it induced a voltage shift in the gating of I_{to1} but not I_{Ks} in canine ventricular myocytes. A second possible mechanism is the so-called "bilayer-couple" hypothesis (31). According to this hypothesis, a positive amphiphile can be preferentially inserted into the inner leaflet of the cell membrane lipid bilayer, thus creating tension in the membrane and producing changes in ion channel function. The effects of C_{12}-G were not consistent with this mechanism, because C_{12}-G exerted its actions from the extracellular side of the cell membrane. Furthermore, onset and washout of the actions of C_{12}-G were rapid (1–2 min), whereas the actions of an amphiphile on membrane channels mediated by the bilayer-couple mechanism take tens of minutes to develop and reverse (31). A third possible mechanism is that an amphiphile may intercalate into lipid bilayers and alter the membrane surface charge. A fourth mechanism is that C_{12}-G can bind to negative external surface charges specifically associated with rKv1.4 or the I_{to1} channel, with the alkyl side chain interacting with neighboring hydrophobic regions to increase the binding stability. Our data can not differentiate between these latter two possibilities. The channel selectivity seen in canine ventricular myocytes could be explained by the existence of channel-specific external surface charges important for C_{12}-G binding. Alternatively, the relationship between external surface charges and the gating apparatus may be different among various channels. Therefore, the same amount of shift in the external surface potential may have different effects on channel gating.

By either mechanism, C_{12}-G caused a positive shift in the external surface potential. This would cause a bias in the electrical field sensed by the voltage sensor controlling rKv1.4 gating. The multiple effects of C_{12}-G on the function of rKv1.4 can be explained by a primary shift in the voltage dependence of channel activation. Our previous mutagenesis experiments suggested that the inactivation of rKv1.4 is mediated by the so-called "N-type" mechanism (32), similar to that described for the Shaker channel (33). It has been shown for the Shaker channel that this inactivation process has little or no intrinsic voltage dependence. The inactivation process derives its apparent voltage dependence from the activation process (33, 34). This is also likely to be the case for rKv1.4 and is consistent with the data in Fig. 4C showing that, upon strong depolarization, when the degree of channel activation approached a plateau (at or above +30 mV) the rate of rKv1.4 inactivation reached a voltage-insensitive minimum. According to this scheme, the voltage dependence of rKv1.4 inactivation and the rate of inactivation in the presence of C_{12}-G exhibited positive shifts similar to those seen with parameters related to channel activation and recovery from inactivation.

The rate of rKv1.4 current decay in the presence of C_{12}-G reached the same voltage-independent asymptote as in the control at strong depolarizations (Fig. 4C). This suggests that C_{12}-G did not influence voltage-independent transitions between the kinetic states of the channel after activation (33, 34). C_{12}-G delayed the time to reach peak current for rKv1.4 or the time to reach plateau current for a deletion mutant

that lost fast inactivation (RHK1Δ3–25), indicating a slowing of the activation process in the presence of C_{12}-G. This is consistent with the notion that a positive shift in the external surface potential (equivalent to a negative shift in the transmembrane electrical field) could reduce the rate constants for channel activation and increase the rate constants for deactivation. However, the C_{12}-G-induced delay in time to peak current persisted at strong depolarizations, even when other parameters (e.g., degree of channel activation and rate of decay) reached the same levels before and after C_{12}-G application. This is expected; because channels had to traverse at least some of the closed states before they could open, the slowing of channel activation in the presence of C_{12}-G would be manifested as a delay in the time to reach peak current no matter how strong the depolarization.

C_{12}-G did not affect the instantaneous outward current-voltage relationship for rKv1.4. It has been suggested that a positive shift in the surface potential around the outer mouth of ion channels can reduce outward currents through the channels by altering the potential profile along the pores (14). Our observation therefore suggests that the charges of the C_{12}-G binding site are probably insulated from the outer mouth of rKv1.4 channels.

External surface charges may comprise several chemical constituents, i.e., head groups of membrane phospholipids, negatively charged amino acids on the extracellular surfaces of membrane proteins, and sialic acids attached to the *N*-glycosylation sites of membrane proteins on the extracellular surface (10). Further experimentation with site-specific mutations is required to identify the importance of each of these components of external surface charges in the effects of C_{12}-G on ion channels and the relationship between these surface charges and the gating apparatus of different ion channels.

Acknowledgments

The authors would like to thank Dr. Andy Tomcofcik at Lederle of American Cyanamid for providing C_{12}-G and its analogues.

References

1. Bell, J. E., and C. Miller. Effects of phospholipid surface charge on ion-conduction in the K^+ channel of sarcoplasmic reticulum. *Biophys. J.* **45:** 279–287 (1984).
2. Hille, B., A. M. Woodhull, and B. I. Shapiro. Negative surface charge near sodium channels of nerve: divalent ions, monovalent ions, and pH. *Philos. Trans. R. Soc. Lond. B Biol. Sci.* **270:**301–318 (1975).
3. Kass, R. S., and D. S. Krafte. Negative surface charge density near heart calcium channels: relevance to block by dihydropyridines. *J. Gen. Physiol.* **89:**629–644 (1987).
4. Kell, M. J., and L. J. DeFelice. Surface charge near the cardiac inward-rectifier channel measured from single-channel conductance. *J. Membr. Biol.* **102:**1–10 (1988).
5. MacKinnon, R., and C. Miller. Functional modification of a Ca^{2+}-activated K^+ channel by trimethyloxonium. *Biochemistry* **28:**8087–8092 (1989).
6. Perozo, E., and F. Bezanilla. Phosphorylation affects voltage gating of the delayed rectifier K^+ channel by electrostatic interactions. *Neuron* **5:**685–690 (1990).
7. Recio-Pinto, E., W. B. Thornhill, D. S. Duch, S. R. Levinson, and B. W. Urban. Neuraminidase treatment modifies the function of electroplax sodium channels in planar lipid bilayers. *Neuron* **5:**675–684 (1990).
8. Sanguinetti, M. C., and N. K. Jurkiewicz. Lanthanum blocks a specific component of I_K and screens membrane surface charge in cardiac cells. *Am. J. Physiol.* **259:**H1881–H1889 (1990).
9. Gilbert, D. L., and G. Ehrenstein. Membrane surface charge. *Curr. Top. Membr. Transp.* **22:**407–421 (1984).
10. Green, W. N., and O. S. Andersen. Surface charges and ion channel function. *Annu. Rev. Physiol.* **53:**341–359 (1991).
11. Hille, B. Modifiers of gating, in *Ionic Channels of Excitable Membranes*. Sinauer Associates, Sunderland, MA, 445–471 (1992).
12. McLaughlin, S. Electrostatic potentials at membrane-solution interfaces. *Curr. Top. Membr. Transp.* **9:**71–144 (1977).
13. Green, W. N., L. B. Weiss, and O. S. Andersen. Batrachotoxin-modified sodium channels in planar lipid bilayers: ion permeation and block. *J. Gen. Physiol.* **89:**841–872 (1987).
14. MacKinnon, R., R. Latorre, and C. Miller. Role of surface electrostatics in the operation of a high-conductance Ca^{2+}-activated K^+ channel. *Biochemistry* **28:**8092–8099 (1989).
15. Gilbert, D. L., and G. Ehrenstein. Effect of divalent cations on potassium conductance of squid axons: determination of surface charge. *Biophys. J.* **9:**447–463 (1969).
16. MacKinnon, R., and C. Miller. Mutant potassium channels with altered binding of charybdotoxin, a pore-blocking peptide inhibitor. *Science (Washington D. C.)* **245:**1382–1385 (1989).
17. Green, W. N., L. B. Weiss, and O. S. Andersen. Batrachotoxin-modified sodium channels in planar lipid bilayers: characterization of saxitoxin- and tetrodotoxin-induced channel closures. *J. Gen. Physiol.* **89:**873–903 (1987).
18. Benoit, E., and J.-M. Dubois. Interactions of guanidinium ions with sodium channels in frog myelinated nerve fibre. *J. Physiol. (Lond.)* **391:** 85–97 (1987).
19. Kirsch, G. E., J. Z. Yeh, J. M. Farley, and T. Narahashi. Interaction of *n*-alkylguanidines with the sodium channels of squid axon membrane. *J. Gen. Physiol.* **76:**315–335 (1980).
20. Schafer, G. On the mechanism of action of hypoglycemia-producing biguanides: a reevaluation and a molecular theory. *Biochem. Pharmacol.* **25:** 2005–2014 (1976).
21. Tseng-Crank, J., G.-N. Tseng, A. Schwartz, and M. A. Tanouye. Molecular cloning and functional expression of a potassium channel cDNA isolated from a rat cardiac library. *FEBS Lett.* **268:**63–68 (1990).
22. Tseng, G.-N., R. B. Robinson, and B. F. Hoffman. Passive properties and membrane currents of canine ventricular myocytes. *J. Gen. Physiol.* **90:** 671–701 (1987).
23. Tseng, G.-N., M. R. Ziai, and A. J. Blume. Modification of the voltage dependence of transient outward current in canine ventricular myocytes. *Circulation* **84:**II-103 (1991).
24. Tseng, G.-N., and J. Tseng-Crank. Differential effects of elevating $[K]_o$ on three transient outward K^+ channels: dependence on channel inactivation mechanism. *Circ. Res.* **71:**657–672 (1992).
25. Bolton, R., N. Dascal, B. Gillo, and Y. Lass. Two calcium-activated chloride conductances in *Xenopus laevis* oocytes permeabilized with the ionophore A23187. *J. Physiol. (Lond.)* **408:**511–534 (1989).
26. Hamill, O. P., A. Marty, E. Neher, B. Sakmann, and F. J. Sigworth. Improved patch-clamp techniques for high resolution current recordings from cells and cell-free membrane patches. *Pfluegers Arch.* **391:**85–100 (1981).
27. Soejima, M., and A. Noma. Mode of regulation of the ACh-sensitive K^+ channel by the muscarinic receptor in rabbit atrial cells. *Pfluegers Arch.* **400:**424–431 (1984).
28. Grahame, D. C. The electrical double layer and the theory of electrocapillarity. *Chem. Rev.* **41:**441–501 (1947).
29. Press, W. H., B. P. Flannery, S. A. Teukolsky, and W. T. Vetterling. *Numerical Recipes. The Art of Scientific Computing*. Cambridge University Press, Cambridge, UK (1986).
30. Hoshi, T., W. N. Zagotta, and R. W. Aldrich. Biophysical and molecular mechanisms of Shaker potassium channel inactivation. *Science (Washington D. C.)* **250:**533–538 (1990).
31. Martinac, B., J. Adler, and C. Kung. Mechanosensitive ion channels of *E. coli* activated by amphipaths. *Nature (Lond.)* **348:**261–263 (1990).
32. Tseng-Crank, J., J.-A. Yao, M. F. Berman, and G.-N. Tseng. Functional role of the NH_2-terminal cytoplasmic domain of a mammalian A-type K^+ channel. *J. Gen. Physiol.* **102:**1057–1083 (1993).
33. Zagotta, W. N., and R. W. Aldrich. Voltage-dependent gating of Shaker A-type potassium channels in *Drosophila* muscle. *J. Gen. Physiol.* **95:** 29–60 (1990).
34. Aldrich, R. W., D. P. Corey, and C. F. Stevens. A reinterpretation of mammalian sodium channel gating based on single channel recording. *Nature (Lond.)* **306:**436–441 (1983).

Send reprint requests to: Gea-Ny Tseng, Department of Pharmacology, Columbia University, 630 West 168th Street, New York, NY 10032.